CHAPTER 7

FERROELECTRIC RELAXOR BEHAVIOUR AND IMPEDANCE SPECTROSCOPY OF B_2O_3-DOPED $BaTi_{0.9}Sn_{0.1}O_3$ CERAMICS

In this study, the B_2O_3 doped $Ba(Ti_{0.9}Sn_{0.1})O_3$ ceramics were prepared by using a solid state reaction method. The perovskite structure was confirmed by using a X-ray diffraction. The fresh surface morphologies were observed by using a scanning electron microscopy (SEM) analysis. The wide range of frequency (0.1 Hz-1MHz) and temperature (20-280 ℃) dependence of the impedance relaxation were investigated. The impedance study indicates the presence of dielectric relaxation both bulk and grain boundary effects in the material. The relaxation times for grain and grain boundary estimated from Col-Cole plots varied with temperature according to the Arrhenius relation. The activation energy for grain and grain boundary were estimated to be 0.73 and 0.85 eV, respectively.

7.1 Introduction

It has been more than a decade since the study focusing on relaxor ferroelectric materials owing to their various modern technological applications. Most of relaxor ferroelectric materials are complex perovskite (ABO_3) structure, for example, $Pb(Mg_{1/3}Nb_{2/3})O_3$(PMN), $Pb(Mg_{1/3}Nb_{2/3})O_3$-PbTiO3 (PMN-PT), $(Bi_{1/2}Na_{1/2})TiO_3$-$BaTiO_3$ (BNT-BT) [1, 2]. The relaxor behavior appears when heterovalent cations are randomly distributed to A or B sites [3]giving rise to random

fields, which tend to cause diffuse phase transition along with the frequency dispersion of phase transition temperature[4].Barium Stannate Titanate ($BaTi_{1-x}Sn_xO_3$) (BTS) is one of the most interesting and extensively studied relaxor materials, which has already shown its immense potential in many microelectronic devices such as bending actuators [5], integrated capacitors with high-permittivity dielectrics [6], multifunctional sensors[7], microwave tunable filters [8] and microwave phase shifters [9]. It is noticed that increasing of Sn content in BTS ceramic decreased the temperature of ferrolectric-paraelectric phase transition and the maximum of dielectric peaks became more diffuse[10-13].Particularly when the Sn concentration is between 10 and 20%, the relaxor-like behavior is observed at temperatures between 0 and 60°C[11, 12]. Thus, these compositions were suitable for the devices which are operated near the room temperatures.

It has been widely accepted that the electrical properties of modified $BaTiO_3$can be tailored by doping some rare earth elements, for instance; doping of Sb_2O_3, $Bi_2O_3$and B_2O_3can enhance the positive temperature coefficient resistance effect of $Ba_{0.88}Sr_{0.12}TiO_3$ ceramics [14-16], and adding small amount of B_2O_3 can improve the remanent polarization of $Ba_{0.7}Sr_{0.3}TiO_3$ ceramic[17]. However, there were a few attempts to transfer the dopants to the compositional of BTS ceramics. The purpose of the present study was to investigate the dielectric response BTS ceramics at different B_2O_3 content. Impedance spectroscopy formalism has been used as a tool to investigate the dielectric relaxation and dynamics of the ionic movement inside the doped BTS ceramics

7.2 Experimental procedure

Polycrystalline $Ba(Ti_{0.9}Sn_{0.1})O_3$ ceramic was prepared by the conventional method. Starting materials were $BaCO_3$, SnO_2, and TiO_2. These powders in stoichiometric proportions were thoroughly mixed and ball-milled in isopropanol for 24 h using zirconia grinding media. After mixing, the slurry was dried, sieved and calcined at 1300°C for 2h in air. The calcined powder was reground with B_2O_3 powder, equivalent to 1.0, 2.0, and 3.0 wt.%. The mixed powders, with the addition of polyvinyl alcohol as an organic binder, were then ball-milled in isopropanol for 24 h. These slurries were dried at 150°C and sieved to form fine powders which were then pressed into pellets with 15 mm diameter under 100 MPa force. The pellets were at last sintered at 1350°C for 4h with a heating/cooling rate of 5°C/min after binder burnout at 500°C for 1h.

Crystalline structures of the sintered samples were checked using a Bruker D8 Advance X-ray diffractometer with a Cu-Kα source. The surface morphologies of the samples were examined using a scanning electron microscopy (SEM). To conduct dielectric and impedance spectroscopy measurement, the pellet specimens were polished and electroded using gold sputtering. The impedance measurements were carried out from 40 to 280°C using a Solartron 1260 Impedance/Gain-phase Analyzer.

7.3 Results and discussion

7.3.1 Structural properties

The microstructures of fresh surface of BTS10 doped with different B_2O_3 content are shown in Figure 7.1. There are some small grains on the grain boundary

for undoped sample, which is similar to Cai's work [9]. They suggested that these small grains occurred due to the segregation of Sn^{4+} ion on grain boundary and hindrance grain growth. It is also observed that most of all sintered BTS ceramics are dense and adding boron oxide can promote liquid phase sintering, however, overdoped B_2O_3 may enhance volatilization and then lead to form large pores in the ceramic. Moreover, the size of ionic radius of B^{3+} ion (0.23 Å) differs very much from that of Ti^{4+} (0.61 Å) and Sn^{4+} (0.69 Å) cations in BTS10 ceramics, thus the solubility of B_2O_3 in BTS10 ceramcis may be limited.

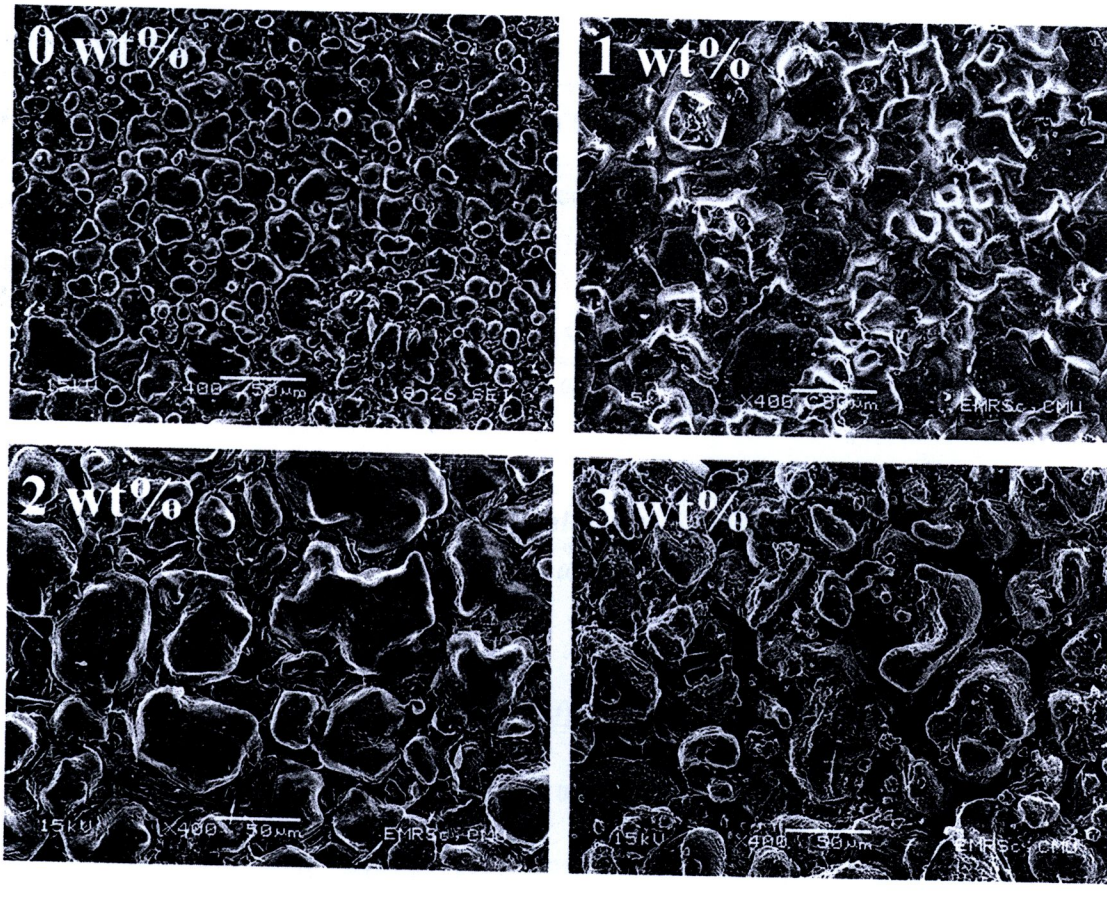

Figure 7. 1 Surface morphology of barium stannate titanate ceramics with different B_2O_3 addition.

7.3.2 Relaxation behavior

Complex impedance spectroscopy analysis is the most commonly used technique to analyze dielectric behavior and dynamics of the ionic movement in electrical materials[18, 19]. Different complex formalism is used to characterize different solids. In many cases, representation of the process was analyzed by more than one of complex formalism to better understand the mechanism. Sometimes the complex impedance (Z^*) plane plots and Debye peak in spectroscopic plots of the imaginary components (Z'') versus $\log f$ are the useful technique for determination of more resistive regions such as grain boundaries and sample surface layers. Whereas the electric modulus (M'') data was found to be a better technique to characterize the contribution of a small capacitance region such as grain interiors [20].The origin of a Debye peak is described by the following equations:

$$Z'' = R\left[\frac{\omega RC}{1+\omega RC^2}\right] \tag{7.1}$$

$$M'' = \frac{\varepsilon_0}{C}\left[\frac{\omega RC}{1+\omega RC^2}\right] \tag{7.2}$$

where ω is the angular frequency ($2\pi f$), C_0 is the vacuum capacitance of the measuring cell and electrodes with an air gap in the place of the sample. The contribution of various microscopic elements such as grain, grain boundary, and electrodes to total dielectric response in polycrystalline materials can be identified by

the reference to an equivalent circuit, which contains a series array of parallel resistor-capacitor (RC) elements [19]. Each individual RC element is differentiated by its unique relaxation time (τ=RC). Therefore, response of these components lies in different time domains [18].

In the present case we have used complex impedance along with the electric modulus formalism to analyze B_2O_3 doped BTS10 ceramics data. Figure 7.2, Figure 7.3 and Figure 7.4 depict the variation of the imaginary part of impedance Z″ as a function of frequency at different temperatures in the 0, 2 and 3 wt.% B_2O_3-doped BTS10 system, respectively.

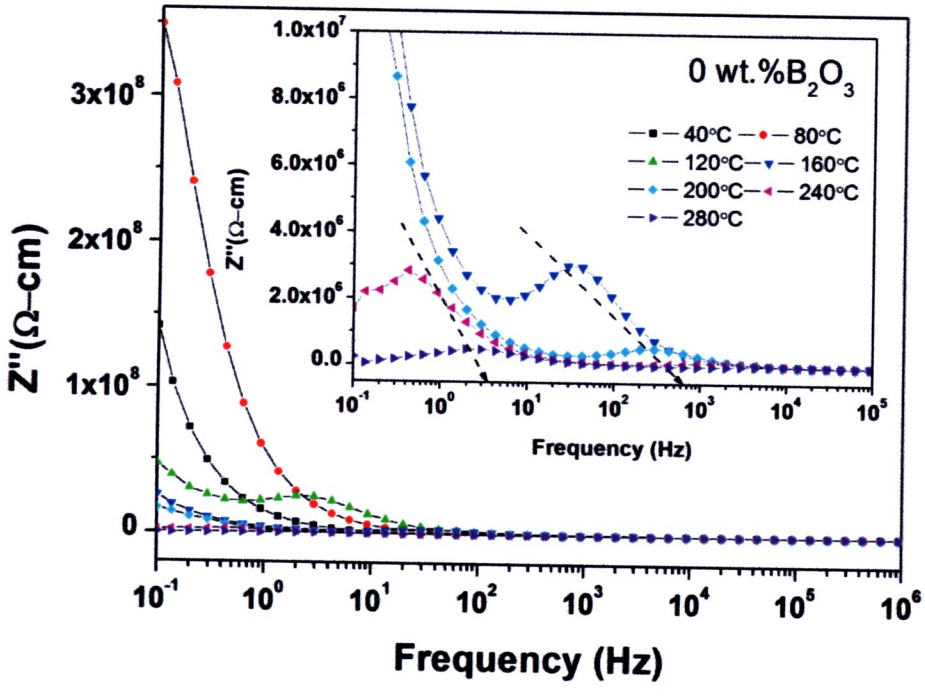

Figure 7. 2 Frequency dependence of imaginary part of complex impedance Z″ for 0wt.%B_2O_3-doped BTS10 ceramic at different temperatures

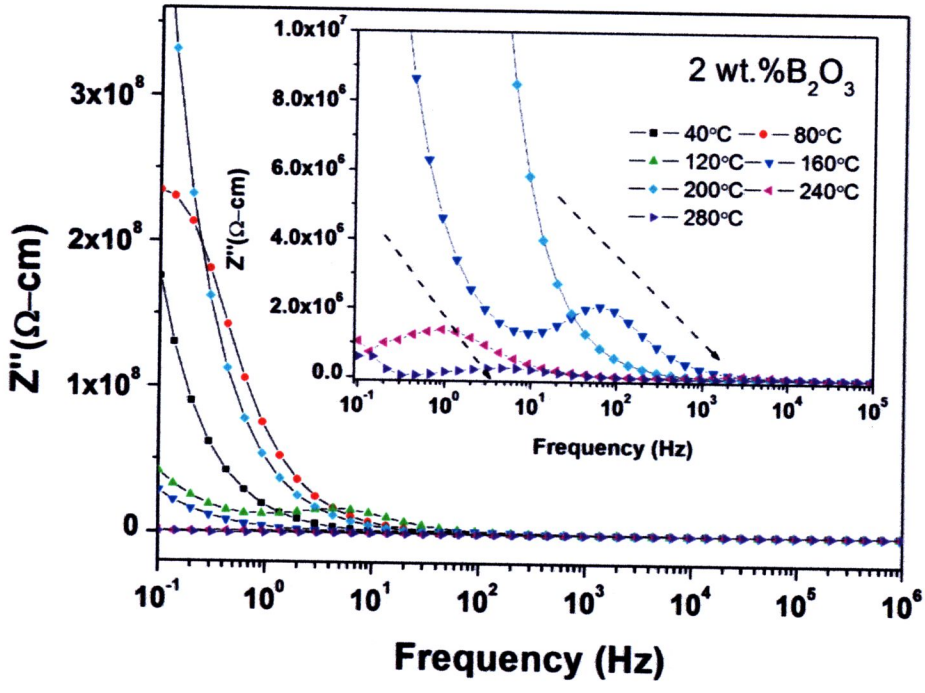

Figure 7. 3 Frequency dependence of imaginary part of complex impedance Z″ for 2wt.%B_2O_3-doped BTS10 ceramic at different temperatures

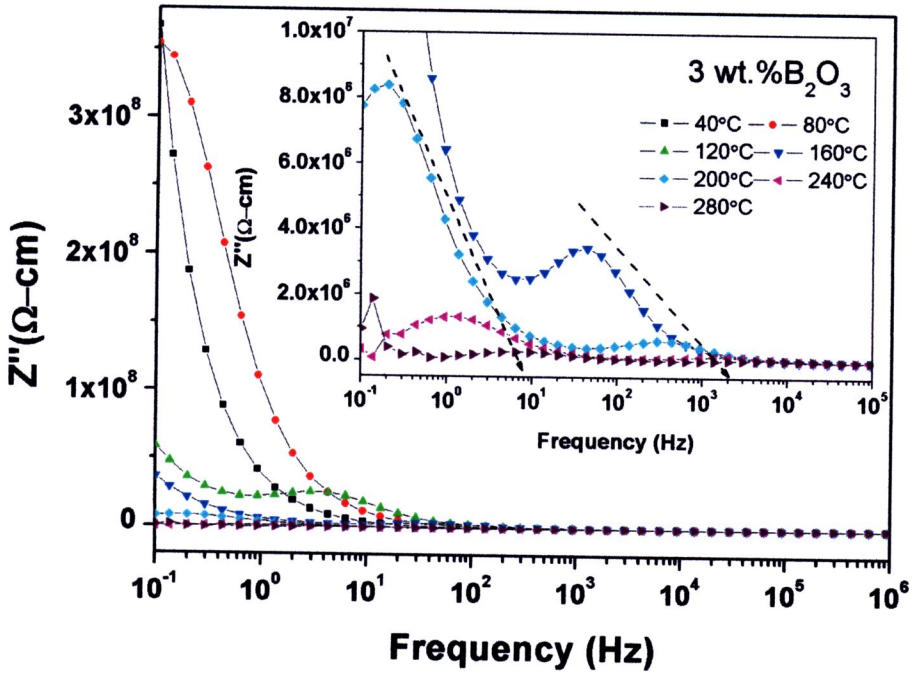

Figure 7. 4 Frequency dependence of imaginary part of complex impedance Z″ for 3wt.%B_2O_3-doped BTS10 ceramic at different temperatures.

From the imaginary part of the impedance Z″ plots, it can be seen that impedance relaxation peak started appearing at temperatures above 120°C for the undoped sample and above 80°C for the doped samples; this behavior is due to the presence of space charges in the material [21]. Moreover, the curves at different temperatures exhibited broad peak maxima (as shown in the inset of Figure 7.4) because of the distribution of relaxation times in the samples. As the temperature increased, the peaks were also observed to shift towards higher frequencies and the magnitude of the Z″decreased with temperature, indicating the multiple relaxations and increasing in loss of the material. Further the merged curve at higher frequencies is the evidence of disappearance of space charge polarization [22, 23].

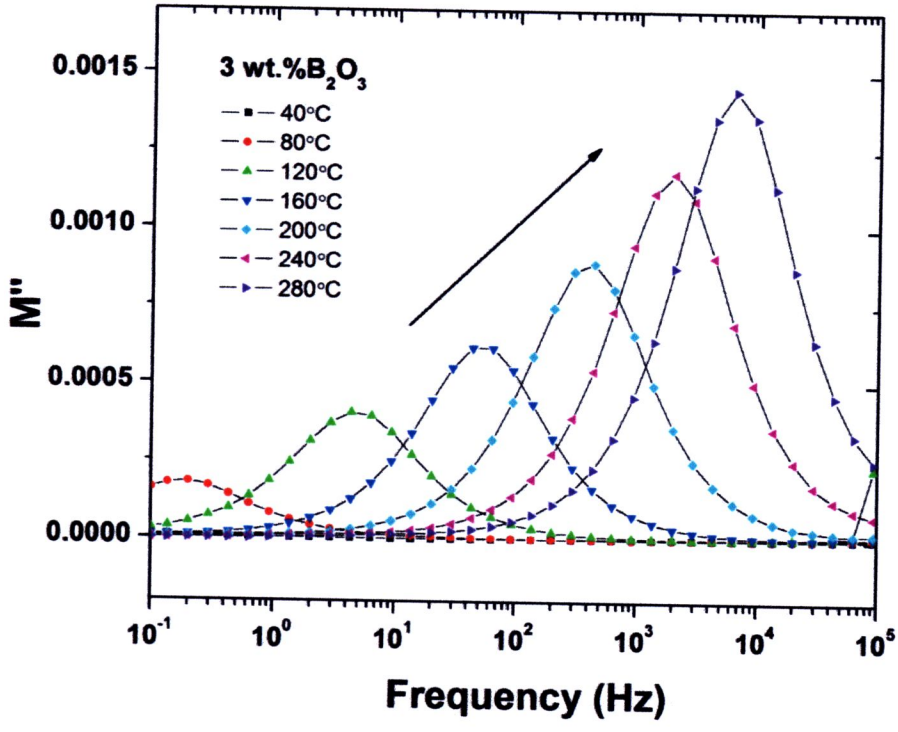

Figure 7. 5 Frequency dependence of imaginary part of electrical modulus M″ for 3wt.%B_2O_3-doped BTS10 ceramic at different temperatures.

The complex modulus formalism is normally used to detect bulk phenomena. Figure 7.5 shows the spectroscopic plots of electric modulus (M') at different temperatures for 3wt.%B_2O_3-doped BTS10 ceramic. Each spectrum showed only a single peak at the low frequency region ($f < 10^4$ Hz) which contribute to the single relaxation process in the grain interior. The peak maxima become narrow and appeared to shift towards the higher frequency region with increasing temperature owing to the distribution of relaxation times in the sample[23].

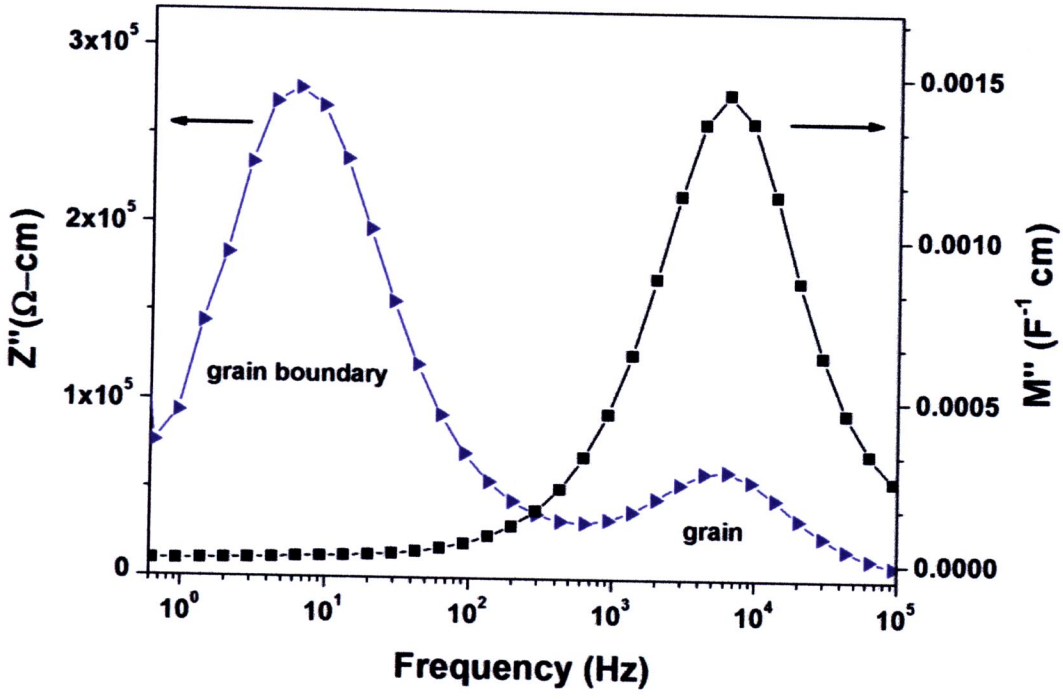

Figure 7. 6 Combined spectroscopic plots of the imaginary components of impedance Z'' and electric modulus M'' for 3wt.%B_2O_3-doped BTS10 ceramic at 280°C.

A typical Z'' and M''versus frequency plot at 280°C for 3wt.%B_2O_3-doped BTS10 ceramic is shown in Figure 7.6. The plots show two peaks in Z'', whereas in

M''only one. The low-frequency Z''spectrum (Z''_{max} at ~6 Hz) was assigned to a grain-boundary response and the high-frequency M''spectrum (M''_{max} at ~ 7 kHz) was assigned to a grain interior response. In the ideal case for each RC element gives rise to a Debye peak, the spectrum of Z'' and M''should be coincident at a particular frequency with a width at half height of 1.14 decades[24]. In the present case, the plots reveal that both peaks of Z'' and $M''$are found to coincide within the high frequency range.

Figure 7.7 shows the complex impedance plane of 3wt.% B_2O_3-doped BTS10 ceramic at temperatures between 280 and 120 °C. It can be seen that the shape of Cole-Cole plots depend on temperature. The slope of the lines decreases with increasing temperature and the curves shift toward Z' axis. According to the literature, the first arc at high-frequency region is ascribed to grain-interior relaxation phenomena, while the second one at low-frequency is the contribution from partial or complete blockings of charge carriers at the grain boundary [25]. From Figure 7.7, the low-frequency arc was not found at <200°C, which may be due to the effect of electrode relaxation process overlapping with the grain boundary relaxation process [10]. However, with the increase of temperature ≥200°C (figure not shown) impedance spectra for all the samples contained two semicircles.

The R and C values can be extracted from these semicircles using an appropriate equivalent circuit. Normally the simplest appropriate equivalent circuit in the case of polycrystalline materials such like $BaTiO_3$-based ceramics is a series array of parallel RC elements [26].

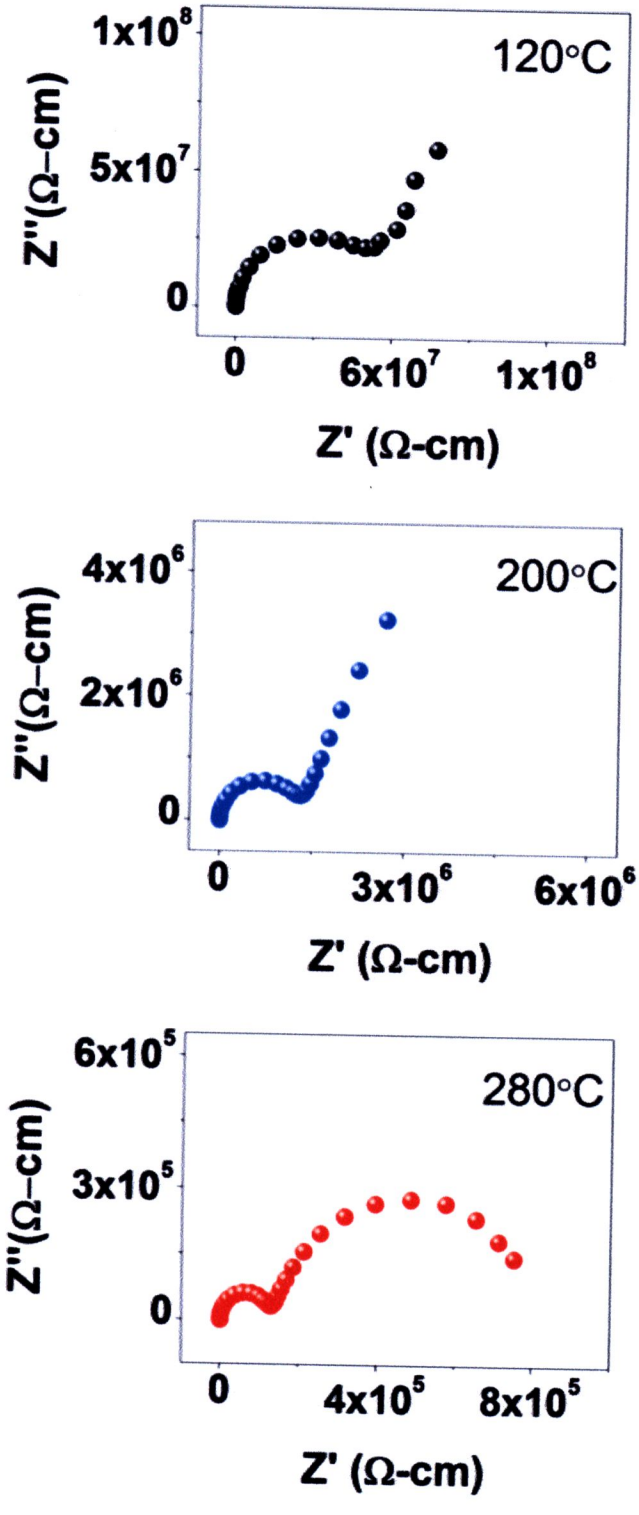

Figure 7. 7 Complex impedance plane plots for 3wt.%B_2O_3-doped BTS10 ceramic at different temperatures.

However, at temperature above the ferroelectric-paraelectric transition, the center of observed plots was below the x-axis then the capacitor can be replaced with constant phase element (CPE) to account for non-Debye behavior [27] as shown in the inset of Figure 7.8.

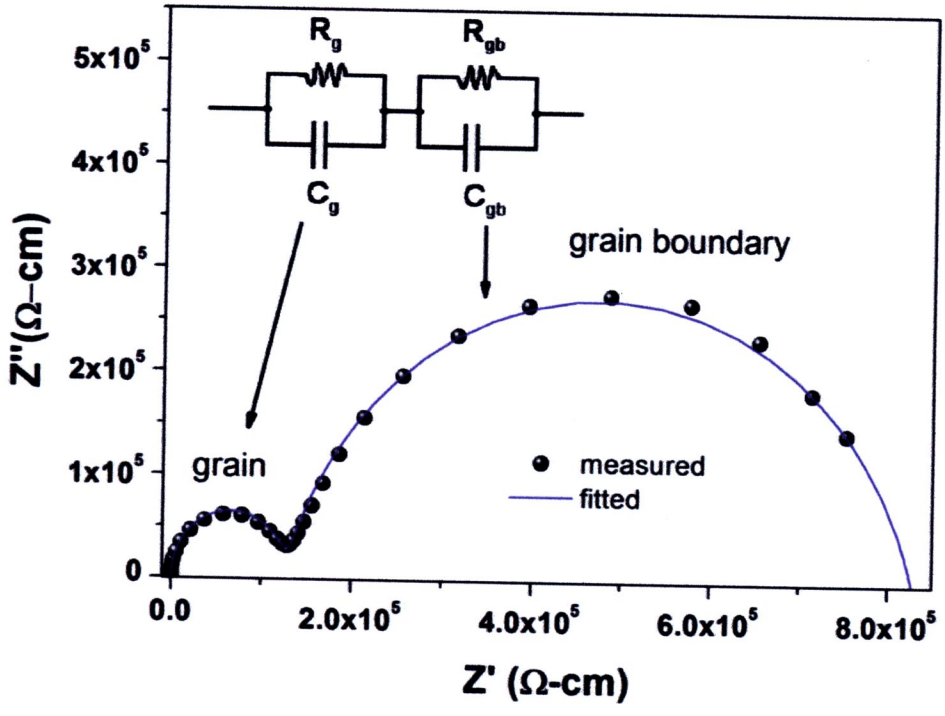

Figure 7. 8 The model of equivalent circuit used for fitting of complex impedance plane plots for 3 wt.%B_2O_3-doped BTS10 ceramic at 280°C.

Figure 7.9 represents the variation of the complex impedance plots with varying concentration of boron oxide in the BTS10 ceramics at temperatures 280°C. The measured data were fitted in computer program Z-View2. It can be seen that the measured data and fitted line are well-matched. Then, the resistance and capacitance at grain and grain boundary for all samples were estimated and reported in Table 7.1.

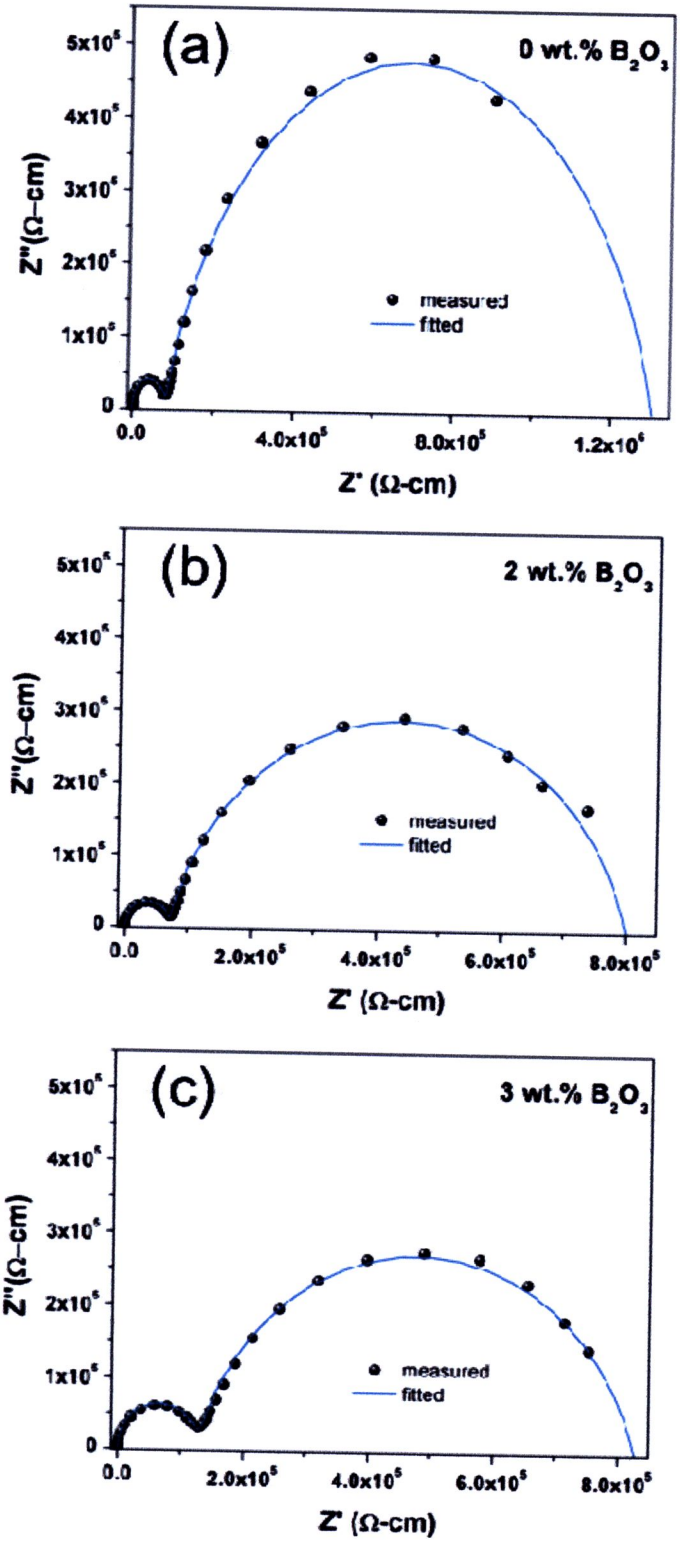

Figure 7. 9 Complex impedance plots for different compositions of B_2O_3 doped-BTS10 ceramics at 280°C.

Table 7. 1Calculated parameters from the Cole-Cole plots at 280°C.

B_2O_3 (wt.%)	R_g (Ω)	C_g (F)	R_{gb}(Ω)	C_{gb} (F)	τ_g (s)	τ_{gb} (s)
0	81005	3.13×10^{-10}	1.224×10^{6}	7.78×10^{-8}	0.99×10^{-5}	9.51×10^{-2}
2	92751	1.26×10^{-10}	1.105×10^{6}	4.34×10^{-8}	1.17×10^{-5}	4.79×10^{-2}
3	124780	2.13×10^{-10}	0.707×10^{6}	6.34×10^{-8}	2.66×10^{-5}	4.49×10^{-2}

The grain boundary contribution decreased for higher boron content, meanwhile, the grain interior contribution slightly increased. The magnitude of C_g is consistent with a bulk ferroelectric response and the magnitude of C_{gb} is consistent with a grain boundary response [28]. The associated relaxation time for grain (τ_g) and grain boundary (τ_{gb}) can also be calculated from the Cole-Cole plots. Normally, the relaxation time is a geometry independent parameter, it does not depend on microstructure but depends only on the intrinsic conductivity of material [29].

Figure 7.10 and Figure 7.11 show the temperature dependence of relaxation time for grain and grain boundary, respectively. From the relaxation times, the activation energies (E_a) for relaxations are calculated using the relation

$$\tau = \tau_0 \, e^{-E_a/k_B T} \tag{7.3}$$

where k_B is the Boltzmann's constant and T is the absolute temperature. It is found that the plots followed the Arrhenius law and the activation energy obtained in these samples is presented in Table 7.2.

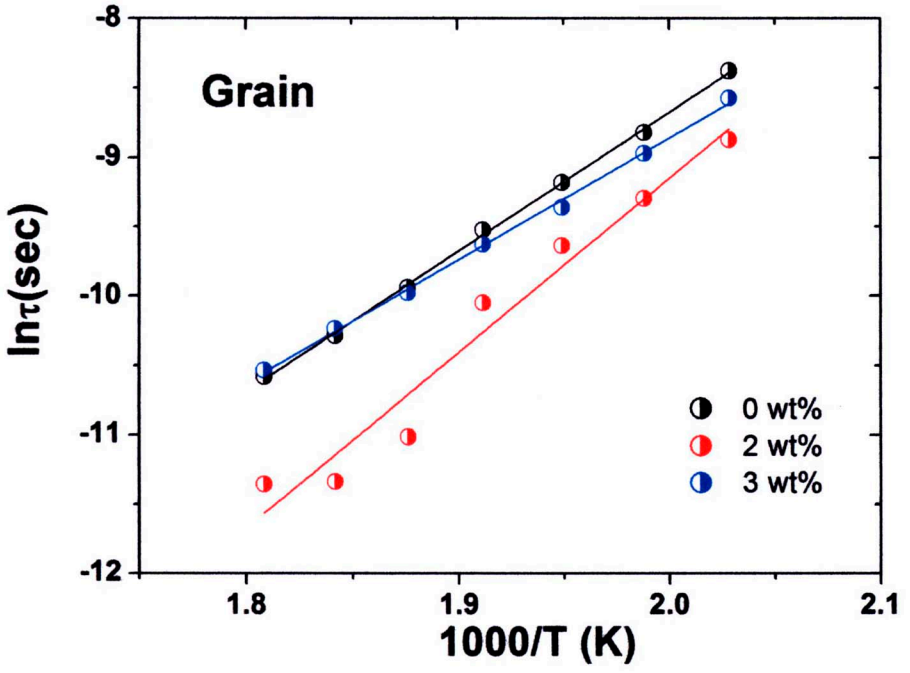

Figure 7. 10 Arrhenius plot of grain relaxation time for B_2O_3-doped BTS10 ceramic at 280°C.

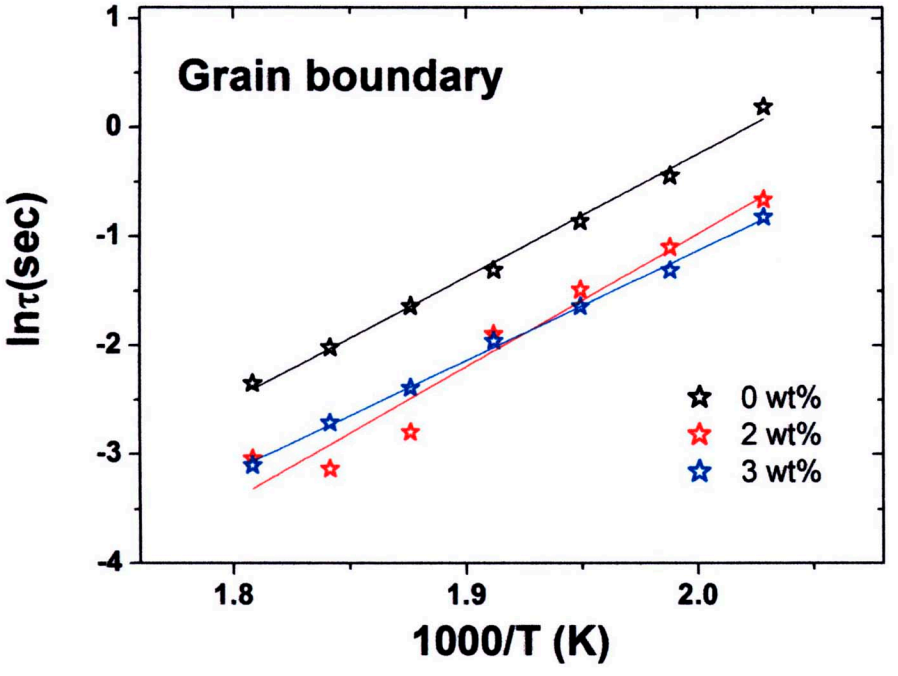

Figure 7. 11 Arrhenius plot of grain boundary relaxation time for B_2O_3-doped BTS10 ceramic at 280°C.

Table 7. 2 Activation energies of B_2O_3 doped-BTS10 ceramics.

B_2O_3 (wt%)	Activation energy (eV)	
	Grain	Grain boundary
0	0.82	0.92
2	1.02	0.99
3	0.73	0.85

These values are similar to those reported by Markovic et al.[27] and Shvartsman et al.[30]. The value of activation energy clearly suggested a possibility that the conduction in the high temperature range was ionic in nature due to oxygen vacancies. In perovskite ferroelectric materials oxygen vacancies are considered one of the mobile charge carriers and mostly in titanates, ionization of oxygen vacancies creates conduction electrons. In our case, activation energy for grain boundaries was more than the grain contribution that showed the resistive nature of the grain boundaries.

7.4 Conclusions

$Ba(Ti_{0.9}Sn_{0.1})O_3$ ceramic doped with B_2O_3 compositions were fabricated by the conventional solid-state route. The perovskite structure of the solid solution was maintained with amount of B_2O_3 concentration. The ferroelectric relaxor behavior in the 3 wt.%B_2O_3-doped BTS10 ceramic was investigated by an IS technique. At high temperature impedance and electric modulus were found to be temperature dependent and showed distributed relaxation phenomena which provided the evidence of typical relaxor properties. The complex impedance plots revealed the existence of grain and

grain boundary contributions. The relaxation time followed Arrhenius behavior and showed different activation energies for grain and grain boundaries.

7.5 References

[1] K.Z.D. Dragan, S. Nava, Dielectric and electromechanical properties of ferroelectric-relaxor 0.9 $Pb(Mg_{1/3}Nb_{2/3})O_3$-0.1$PbTiO_3$ thin films, Journal of Applied Physics, 90 (2001) 4682-4689.

[2] T. Takenaka, H. Nagata, Y. Hiruma, Y. Yoshii, K. Matumoto, Lead-free piezoelectric ceramics based on perovskite structures, Journal of Electroceramics, 19 (2007) 259-265.

[3] L.E. Cross, Relaxor ferroelectrics, Ferroelectrics, 76 (1987) 241-267.

[4] V. Westphal, W. Kleemann, M.D. Glinchuk, Diffuse phase transitions and random-field-induced domain states of the ``relaxor'' ferroelectric $PbMg_{1/3}Nb_{2/3}O_3$, Physical Review Letters, 68 (1992) 847.

[5] R. Steinhausen, A. Kouvatov, H. Beige, H.T. Langhammer, H.P. Abicht, Poling and bending behavior of piezoelectric multilayers based on $Ba(Ti,Sn)O_3$ ceramics, Journal of the European Ceramic Society, 24 (2004) 1677-1680.

[6] C. Pientschke, A. Kouvatov, R. Steinhausen, W. Seifert, H. Beige, Polarisation kinetics of electrically connected electroconductive ferroelectric multilayer structures, Journal of the European Ceramic Society, 25 (2005) 2547-2551.

[7] S.-J. Lee, H.-C. Ryu, J. Moon, Y.-H. Song, T. Zyung, Structural and dielectric properties of barium stannate titanate thin films for microwave tunable devices and multifunctional sensors, Integrated Ferroelectrics, 93 (2007) 141-147.

[8] S.N. Song, J.W. Zhai, X. Yao, Dielectric and microwave properties of $Ba(Sn_{0.15}Ti_{0.85})O_3$ thin films, Materials Letters, 62 (2008) 1173-1175.

[9] W. Cai, Y. Fan, J. Gao, C. Fu, X. Deng, Microstructure, dielectric properties and diffuse phase transition of barium stannate titanate ceramics, Journal of Materials Science: Materials in Electronics, 22 (2011) 265-272.

[10] S. Markovic, M. Mitric, N. Cvjeticanin, D. Uskokovic, Preparation and properties of $BaTi_{1-x}Sn_xO_3$ multilayered ceramics, Journal of the European Ceramic Society, 27 (2007) 505-509.

[11] V.V. Shvartsman, J. Dec, Z.K. Xu, J. Banys, P. Keburis, W. Kleemann, Crossover from ferroelectric to relaxor behavior in $BaTi_{1-x}Sn_xO_3$ solid solutions, Phase Transitions, 81 (2008) 1013-1021.

[12] X. Wei, X. Yao, Preparation, structure and dielectric property of barium stannate titanate ceramics, Materials Science and Engineering: B, 137 (2007) 184-188.

[13] N. Baskaran, H. Chang, Effect of Sn doping on the phase transformation properties of ferroelectric $BaTiO_3$, Journal of Materials Science: Materials in Electronics, 12 (2001) 527-531.

[14] J. Qi, Z. Gui, Y. Wu, L. Li, Enhancement of PTCR effect of semiconducting $Ba_{1-x}Sr_xTiO_3$ by Sb_2O_3 vapor, Sensors and Actuators A: Physical, 93 (2001) 84-85.

[15] J. Qi, W. Chen, Y. Wu, L. Li, Improvement of the PTCR effect in $Ba_{1-x}Sr_xTiO_3$ semiconducting ceramics by doping of Bi_2O_3 vapor during sintering, Journal of the American Ceramic Society, 81 (1998) 437-438.

[16] Q. Jianquan, Z. Qing, W. Yongli, W. Yajing, L. Longtu, Enhancement of positive temperature coefficient resistance effect of $BaTiO_3$-based semiconducting ceramics caused by B_2O_3 vapor dopants, Solid State Communications, 120 (2001) 505-508.

[17] S.M. Rhim, S. Hong, H. Bak, O.K. Kim, Effects of B_2O_3 addition on the dielectric and ferroelectric properties of $Ba_{0.7}Sr_{0.3}TiO_3$ ceramics, Journal of the American Ceramic Society, 83 (2000) 1145-1148.

[18] A. Laha, S.B. Krupanidhi, Dielectric response and impedance spectroscopy of $0.7Pb(Mg_{1/3}Nb_{2/3})O_3$-$0.3PbTiO_3$ thin films, Materials Science and Engineering B, 98 (2003) 204-212.

[19] S.D. C., W.A. R., Impedance and modulus spectroscopy of semiconducting $BaTiO_3$ showing positive temperature coefficient of resistance, Journal of Applied Physics, 66 (1989) 3850-3856.

[20] F.D. Morrison, D.C. Sinclair, A.R. West, Characterization of lanthanum-doped barium titanate ceramics using impedance spectroscopy, Journal of the American Ceramic Society, 84 (2001) 531-538.

[21] A.R. James, K. Srinivas, Low temperature fabrication and impedance spectroscopy of PMN-PT ceramics, Materials Research Bulletin, 34 (1999) 1301-1310.

[22] E.V. Ramana, S.V. Suryanarayana, T.B. Sankaram, ac impedance studies on ferroelectromagnetic $SrBi_{5-x}La_xTi_4FeO_{18}$ ceramics, Materials Research Bulletin, 41 (2006) 1077-1088.

[24] J.R. Macdonald, Impedance spectroscopy : emphasizing solid materials and systems, : Wiley, New York, 1987.

[25] V. Prashanth Kumar, Y.S. Reddy, P. Kistaiah, G. Prasad, C. Vishnuvardhan Reddy, Thermal and electrical properties of rare-earth co-doped ceria ceramics, Materials Chemistry and Physics, 112 (2008) 711-718.

[26] A.R. West, D.C. Sinclair, N. Hirose, Characterization of electrical materials, especially ferroelectrics, by impedance spectroscopy, Journal of Electroceramics, 1 (1997) 65-71.

[27] S. Marković, Č. Jovalekić, L. Veselinović, S. Mentus, D. Uskoković, Electrical properties of barium titanate stannate functionally graded materials, Journal of the European Ceramic Society, 30 (2010) 1427-1435.

[28] J.T.S. Irvine, D.C. Sinclair, A.R. West, Electroceramics: characterization by impedance spectroscopy, Advanced Materials, 2 (1990) 132-138.

[29] P. Sooksaen, I. Reaney, D. Sinclair, Crystallization and dielectric properties of borate-based ferroelectric $PbTiO_3$; glass-ceramics, Journal of Electroceramics, 19 (2007) 221-228.

[30] V.V. Shvartsman, Diffuse phase transition in $BaTi_{1-x}Sn_xO_3$ ceramics: An intermediate state between ferroelectric and relaxor behavior, J. Appl. Phys., 99 (2006) 124111.